

Atomic hydrogen scaling relations at $z \approx 0.35$

APURBA BERA,^{1,2,3} NISSIM KANEKAR,² JAYARAM N. CHENGALUR,² AND JASJEET S. BAGLA⁴

¹*International Centre for Radio Astronomy Research, Curtin University, Bentley, WA 6102, Australia*

²*National Centre for Radio Astrophysics, Tata Institute of Fundamental Research, Pune 411007, India*

³*Inter-University Centre for Astronomy and Astrophysics, Pune 411007, India*

⁴*Indian Institute of Science Education and Research Mohali, Knowledge City, Sector 81, Sahibzada Ajit Singh Nagar, Punjab 140306, India*

ABSTRACT

The atomic hydrogen (HI) properties of star-forming galaxies in the local Universe are known to correlate with other galaxy properties via the “HI scaling relations”. The redshift evolution of these relations serves as an important constraint on models of galaxy evolution. However, until recently, there were no estimates of the HI scaling relations at cosmological distances. Using data from a deep Giant Metrewave Radio Telescope HI 21 cm survey of the Extended Groth Strip, and the technique of spectral line stacking, we determine the scaling relation between the HI mass and the stellar mass for star-forming galaxies at $z \approx 0.35$. We use this measurement, along with the main-sequence relation in galaxies, to infer the dependence of the HI depletion timescale of these galaxies on their stellar mass. We find that massive star-forming galaxies at $z \approx 0.35$, with stellar mass $M_* \gtrsim 10^{9.5} M_\odot$, are HI-poor compared to local star-forming galaxies of a similar stellar mass. However, their characteristic HI depletion time is lower by a factor of ≈ 5 than that of their local analogues, indicating a higher star-formation efficiency at intermediate redshifts (similar to that at $z \approx 1$). While our results are based on a relatively small cosmic volume and could thus be affected by cosmic variance, the short characteristic HI depletion timescales ($\lesssim 3$ Gyr) of massive star-forming galaxies at $z \approx 0.35$ indicate that they must have acquired a significant amount of neutral gas through accretion from the circumgalactic medium over the past four Gyr, to avoid quenching of their star-formation activity.

Keywords: Galaxy evolution — Radio spectroscopy — Neutral atomic hydrogen

1. INTRODUCTION

The atomic hydrogen (HI) reservoir of galaxies provides the primary fuel reservoir for star-formation activity, and is thus a critical factor in galaxy evolution. While star-formation takes place in the molecular phase and the exact role of HI in galaxy evolution is not clearly understood, the lack of HI in red quenched galaxies in the local Universe suggests that the exhaustion of the HI reservoir leads to the suppression, and subsequent quenching, of the star-formation activity in galaxies (e.g. [Saintonge & Catinella 2022](#)). Conversely, HI has been detected in a significant fraction ($\approx 40\%$) of early-type galaxies in the Atlas3D sample (e.g. [Serra et al. 2012](#)), indicating that the conversion of HI to stars is likely to be affected by several factors (e.g. [Davis et al. 2014](#)). Measurements of the HI content of galaxies via HI 21 cm spectroscopy have hence long been of much interest in probing galaxy evolution.

In the nearby Universe, the HI properties of star-forming galaxies are known to correlate with their stellar properties¹, through the HI scaling relations (e.g. [Toribio et al. 2011](#); [Dénes et al. 2014](#); [Wang et al. 2016](#)). These include relations between the HI mass, M_{HI} , and the stellar mass, M_* (e.g. [Catinella et al. 2018](#); [Parkash et al. 2018](#)), the HI mass and different optical magnitudes (e.g. [Dénes et al. 2014](#)), the HI mass and the HI size (e.g. [Broeils & Rhee 1997](#); [Wang et al.](#)

Corresponding author: Nissim Kanekar
nkanekar@ncra.tifr.res.in

¹ Note that the correlations typically have significantly higher scatter for volume-limited samples that contain both star-forming and passive galaxies (see, e.g., [Parkash et al. 2018](#)).

2016), etc. Such relations provide a critical constraint on numerical and semi-analytical models of galaxy evolution (e.g. Davé et al. 2020).

Unfortunately, the intrinsic faintness of the HI 21 cm transition has meant that there have been few detections of HI 21 cm emission from individual galaxies at $z \gtrsim 0.25$ (e.g. Catinella & Cortese 2015; Fernández et al. 2016; Gogate et al. 2020). Further, even these detections have only been in the most massive galaxies; this has meant that we have had no information about HI scaling relations beyond the local Universe. Recently, the HI 21 cm stacking technique has provided a unique way to statistically measure the average HI properties of a population of galaxies (e.g. Zwaan 2000; Chengalur et al. 2001; Jaffé et al. 2016; Bera et al. 2019; Chowdhury et al. 2021, 2022a). This has made it possible to measure the HI scaling relations for cosmologically-distant galaxies, at both intermediate ($z \approx 0.4$; Bera et al. 2022; Sinigaglia et al. 2022) and moderately-high ($z \approx 1$; Chowdhury et al. 2022b) redshifts. In this *Letter*, we report a measurement of the $M_{\text{HI}} - M_*$ scaling relation in star-forming galaxies at $z \approx 0.35$, based on deep Giant Metreware Radio Telescope (GMRT) HI 21 cm spectroscopy of the Extended Groth Strip (EGS). Comparing our measurement to the known scaling relation in the local Universe, we quantify the evolution of the HI reservoir and the HI depletion timescale (and thus, the star-formation efficiency) of galaxies over the past four Gyr.²

2. OBSERVATIONS AND DATA PROCESSING

We used the GMRT Band-5 receivers to carry out a ≈ 350 -hr observation of the EGS between March 2017 and June 2019, in proposals 31_038 (P.I.: J. S. Bagla), 34_083 (P.I.: N. Kanekar), 35_085 (P.I.: A. Bera), and 36_064 (P.I.: A. Bera). The observations and data analysis are described in detail by Bera et al. (in prep.); a brief summary is provided below.

We used the GMRT Wideband Backend as the correlator for our observations of the EGS, with a bandwidth of 400 MHz covering the frequency range 970 – 1370 MHz, and sub-divided into 8,192 spectral channels. The initial data editing, gain calibration, and bandpass calibration were carried out in the classic AIPS package (Greisen 2003), following standard procedures. Imaging and self-calibration were carried out independently for each observing cycle, and the inferred antenna-based gains applied to the spectral-line visibilities. For each cycle, the model visibilities corresponding to the continuum image of the cycle were then subtracted out from the calibrated spectral-line visibilities. The residual visibilities were then imaged, again independently for each cycle, using the task TCLEAN in the CASA package (version 5.6; McMullin et al. 2007) to make the final spectral cubes. We emphasize that independent spectral cubes were made for each observing cycle; this was done to ensure that any low-level radio frequency interference (RFI) in a given cycle would not affect the data from the other cycles. The cubes were made in the barycentric frame, using w-projection (Cornwell et al. 2008) and Briggs weighting with ROBUST=0.5 (Briggs 1995), and were corrected for the frequency-dependent shape of the GMRT primary beam. The FWHM of the GMRT primary beam is $\approx 28' - 34'$ over the frequency range 1184 – 1000 MHz, corresponding to a spatial scale of $\approx 5.5 - 11.3$ Mpc over the redshift range $z = 0.20 - 0.42$. The cubes have a frequency resolution of 97.7 kHz, equivalent to a velocity resolution of $\approx 21 - 30$ km s⁻¹ across the observing band. The native angular resolutions of the cubes (i.e. the FWHMs of the synthesized beams) are $\approx 2''.6 - 3''.3$, corresponding to spatial resolutions of $\approx 9 - 18$ kpc for the redshift range $z = 0.20 - 0.42$.

3. HI 21 cm STACKING ANALYSIS

3.1. The galaxy sample

HI 21 cm stacking experiments critically require a large sample of galaxies within the telescope primary beam, with accurately measured positions and redshifts (e.g. Chowdhury et al. 2022a). The redshift accuracy needs to be significantly better than the typical HI 21 cm line width in order to properly align the line emission from the different galaxies; this implies a required redshift accuracy of $\lesssim 100$ km s⁻¹ (e.g. Maddox et al. 2013). Our target field, the EGS, has excellent spectroscopic coverage from the DEEP2 and DEEP3 surveys (Newman et al. 2013; Cooper et al. 2012), which provide spectroscopic redshifts (accurate to $\lesssim 62$ km s⁻¹, for redshift quality code $Q \geq 3$) for a large number of galaxies with $R_{\text{AB}} \leq 24.1$. The DEEP2 and DEEP3 spectroscopic redshift catalogues are $\approx 60\%$ complete at the limiting apparent magnitude $R_{\text{AB}} = 24.1$ for $Q \geq 3$ (see Fig. 32 of Newman et al. 2013). Most of the incompleteness arises from galaxies with faint emission lines, which are likely to lie at $z > 1.4$ (Newman et al. 2013). However, we

² Throughout this work, we use a flat Λ -cold dark matter (Λ CDM) cosmology, with $(H_0, \Omega_m, \Omega_\Lambda) = (70 \text{ km s}^{-1} \text{ Mpc}^{-1}, 0.3, 0.7)$. All magnitudes in this work are in the AB system (Oke 1974).

note that it is possible that low-redshift galaxies with faint optical emission lines (e.g. obscured, dusty galaxies) might also be missing from our sample.

The parent sample for our HI 21 cm stacking experiment was selected from the combined catalogue of the DEEP2 and the DEEP3 surveys³. The redshift range of our sample was restricted to $0.20 \leq z \leq 0.42$; the upper limit is determined by the frequency coverage of the GMRT Band-5 receivers, and the lower limit by the DEEP2 and DEEP3 redshift coverage. The sample was further restricted to the 808 galaxies which (1) lie within the FWHM of the uGMRT primary beam at the redshifted HI 21 cm line frequency⁴, (2) have reliable redshift estimates (quality code ≥ 3 ; Newman et al. 2013), and (3) have absolute B-band magnitudes of $M_B \leq -16$.⁵ The cosmic volume occupied by our galaxy sample is $\approx 4.7 \times 10^4$ comoving Mpc³.

Next, the presence of an active galactic nucleus (AGN) in a galaxy may affect its HI properties. Outflows driven by AGNs may reduce the HI mass of the AGN host galaxies (e.g. Rupke & Veilleux 2011; Morganti et al. 2016). Further, the HI 21 cm emission spectra of the AGN hosts may also have associated HI 21 cm absorption features which could reduce the stacked HI 21 cm emission signal (e.g. Morganti & Oosterloo 2018; Aditya & Kanekar 2018). We hence excluded 84 galaxies identified as AGN hosts from the stacking sample, based on either their optical spectra (Cooper et al. 2012), or a detection in our radio continuum image with $L_{1.4 \text{ GHz}} \geq 2 \times 10^{23} \text{ W Hz}^{-1}$ (as 1.4 GHz radio luminosities above this threshold predominantly arise from radio-loud AGNs; Condon et al. 2002; Smolčić et al. 2008). Finally, we restricted our sample to blue star-forming galaxies, by excluding 101 “red” galaxies, with $(U - B) + 0.032 (M_B + 21.62) - 1.035 > 0$ (Willmer et al. 2006; Coil et al. 2008). Our final sample contains 623 blue star-forming galaxies at $z = 0.20 - 0.42$.

The stellar masses of the 623 galaxies were estimated from their $U - B$ colours, absolute B-band magnitudes (M_B), and redshifts (z), using the relation

$$\log(M_*/M_\odot) = 1.39(U - B) - 0.44 M_B - 2.10 z + 0.84, \quad (1)$$

derived following Weiner et al. (2009). This relation was calibrated for 127 blue star-forming galaxies (excluding AGN hosts) that are present in both the DEEP2/DEEP3 catalogues and the CANDELS catalogue (Stefanon et al. 2017); the CANDELS stellar mass estimates were used as reference values in the calibration (see Bera et al. in prep., for details). We note that, for the 127 galaxies that were used to calibrate the relation, the RMS scatter between the stellar masses estimated using this relation and the CANDELS stellar mass estimates is 0.16 dex. Star-formation rate (SFR) estimates based on H_α and H_β line luminosities for 309 of the 623 galaxies of our sample were provided by Benjamin J. Weiner, based on DEEP2 spectroscopy⁶. The above SFR estimates are entirely consistent with the (redshift-dependent) main-sequence relation between stellar mass and SFR given by Whitaker et al. (2012),

$$\log(\text{SFR}) = \alpha(\log M_* - 10.5) + \beta \quad (2)$$

where α and β vary with redshift as

$$\alpha(z) = 0.70 - 0.13z, \text{ and } \beta(z) = 0.38 + 1.14z - 0.19z^2.$$

We hence used the above main-sequence relation to estimate the SFRs of all 623 galaxies in our sample from their stellar mass estimates; the error on the SFRs is ≈ 0.25 dex, the scatter in the above main-sequence relation for blue star-forming galaxies (Whitaker et al. 2012). We emphasize that these SFRs are estimated from the stellar mass estimates using the main-sequence relation, and are not independent estimates.

3.2. HI 21 cm subcubes of the sample galaxies

For each galaxy in our sample, a subcube centred at its sky position and redshifted HI 21 cm line frequency was extracted from each of the four spectral data cubes (corresponding to the four observing cycles). The four subcubes obtained for each galaxy were treated independently in our analysis to ensure that any systematic errors in one of the observing cycles would not affect the subcubes from other cycles (e.g. Chowdhury et al. 2022a). Using the

³ <http://deep.ps.uci.edu/deep3>

⁴ This was done because systematic effects in the spectral data cubes are often significant outside the FWHM of the primary beam.

⁵ This M_B limit was chosen to exclude very faint galaxies from our sample. These galaxies are expected to have low HI masses compared to the HI mass of luminous galaxies (based on the $M_{\text{HI}} - M_B$ relation; Dénes et al. 2014); retaining them in the sample would thus significantly reduce the signal-to-noise ratio of the stacked HI 21 cm emission signal.

⁶ Note that these estimates were obtained following the prescriptions of Hopkins et al. (2003), and do not include a correction for dust extinction.

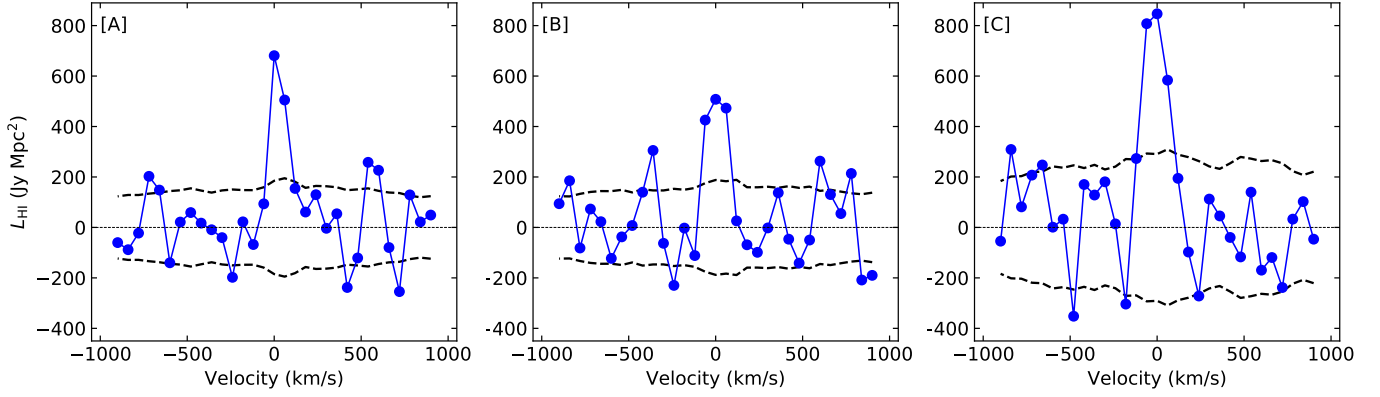


Figure 1. The stacked HI 21 cm emission spectra (in units of luminosity density) for blue galaxies in three (logarithmic) stellar mass bins, [A] $8.00 \leq \log(M_*/M_\odot) < 8.70$, [B] $8.70 \leq \log(M_*/M_\odot) < 9.45$, and [C] $9.45 \leq \log(M_*/M_\odot) \leq 10.40$. The dashed black curves in each panel show the RMS noise in the corresponding velocity planes of the stacked spectral cubes. See text for discussion.

luminosity distance, $d_L(z)$, for each galaxy, each subcube was converted from observed flux density (F_ν , in Jy) to spectral luminosity density (L_{HI} , in Jy Mpc^2), via the relation $L_{\text{HI}} = 4\pi F_\nu d_L^2(z)/(1+z)$.

Next, the optimal spatial resolution for the stacking analysis was chosen such that coarser spatial resolutions yield a stacked HI 21 cm emission signal consistent with that obtained at the optimal resolution. We found that the optimum spatial resolution for our sample is 30 kpc (see Bera 2021; Bera et al. in prep., for detailed discussions). Each subcube was convolved with a Gaussian beam to a (resultant) spatial resolution of 30 kpc at the redshift of the target galaxy, with appropriate normalization to ensure flux conservation (i.e. by ensuring that the peak of the resultant point spread function is unity, after convolving with the same kernel; Chowdhury et al. 2022a). Each subcube was then interpolated, spatially and spectrally, to a pixel size of 5 kpc (at the galaxy redshift) and a velocity resolution of 30 km s^{-1} . A second-order polynomial was then fitted to, and subtracted from, the spectrum at each spatial pixel of each subcube, excluding the central $\pm 200 \text{ km s}^{-1}$ from the fit. The final subcubes cover a spatial range of $500 \text{ kpc} \times 500 \text{ kpc}$, and a velocity range of $\pm 1000 \text{ km s}^{-1}$, at the redshift of each galaxy.

A set of statistical tests were next performed on each subcube to test for the presence of systematic effects (due to, e.g., RFI, deconvolution errors, etc.). Subcubes that showed evidence of such systematics were excluded from the sample.

Finally, 14 galaxies with “close neighbours” were identified and excluded from the sample to reduce the possible effects of source confusion on our results. A “close neighbour” was defined as any galaxy with $M_B \leq -16$ within 30 kpc and $\pm 300 \text{ km s}^{-1}$ of the target galaxy. Our final sample for the stacking analysis consisted of 464 unique galaxies with 1665 subcubes, at a median redshift of $z_{\text{med}} = 0.35$.

3.3. The HI 21 cm stacking procedure

To determine the $M_{\text{HI}} - M_*$ relation at $z \approx 0.35$, we first divided the full galaxy sample into three independent (logarithmic) stellar mass bins. The number of stellar mass bins and the bin widths were selected to ensure that the average HI 21 cm emission signal is detected at $> 4\sigma$ significance in each bin. The stacking of the HI 21 cm emission signals was carried out independently for each stellar mass bin, by stacking the subcubes of all galaxies in the bin, plane-by-plane, with equal weights for all subcubes; this yielded a stacked spectral cube for each bin. A second-order polynomial was then fitted to, and subtracted out from, the spectrum at each spatial pixel of the three stacked cubes, again excluding the central $\pm 200 \text{ km s}^{-1}$. The three residual stacked cubes were then Hanning-smoothed to, and resampled at, a velocity resolution of 60 km s^{-1} . For each stellar-mass bin, the final stacked spectrum was extracted at the central spatial pixel of the corresponding stacked cube.

The stacked HI 21 cm spectra for the three stellar-mass bins are shown in Figure 1; the stacked HI 21 cm emission signal is detected at $> 4\sigma$ significance in all three bins. The average HI 21 cm line luminosity for each bin was determined by integrating the stacked HI 21 cm spectrum over all contiguous central spectral channels with $\geq 1.5\sigma$ significance. For each bin, the RMS noise values measured from each plane of the spectral channels that were identified

Table 1. The average HI mass of blue galaxies in different (logarithmic) stellar mass bins.

log (M_*/M_\odot) range	Number of galaxies	Median M_* $10^9 M_\odot$	$\int L_{\text{HI}} dv$ $10^5 \text{ Jy Mpc}^2 \text{ km s}^{-1}$	$\langle M_{\text{HI}} \rangle$ $10^9 M_\odot$
[8.00 – 8.70]	198	0.26	0.71 ± 0.16	1.33 ± 0.32
[8.70 – 9.45]	174	1.00	0.84 ± 0.19	1.57 ± 0.41
[9.45 – 10.40]	67	6.75	1.34 ± 0.31	2.50 ± 0.69

For each stellar-mass bin, the columns are (1) the stellar mass range, (2) the number of galaxies, (3) the median stellar mass, (4) the velocity-integrated stacked HI 21 cm line luminosity, and (5) the average HI mass. The quoted errors on the velocity-integrated HI 21 cm line luminosities are measurement errors, while those on the HI mass are jackknife errors.

as “line” channels in the corresponding stacked HI 21 cm cube were combined to determine the measurement error, to estimate the detection significance of the average HI 21 cm signal. The average HI mass of the galaxies in each stellar-mass bin was estimated from the corresponding stacked HI 21 cm line luminosity via the relation

$$\frac{M_{\text{HI}}}{M_\odot} = 1.86 \times 10^4 \times \frac{\int L_{\text{HI}} dv}{\text{Jy Mpc}^2 \text{ km s}^{-1}}. \quad (3)$$

Jackknife re-sampling was used to estimate the uncertainties on the average HI masses. The jackknife errors are larger than the measurement errors, and include contributions from both sample variance and any underlying systematic effects. The average HI masses and associated uncertainties are listed in Table 1, along with the stellar mass ranges and the velocity-integrated HI 21 cm line luminosities for each bin. In passing, we note that slight changes in the stellar-mass ranges of the three bins were found to have no significant effect on the inferred scaling relation.

4. THE $M_{\text{HI}} - M_*$ SCALING RELATION AT $Z \approx 0.35$

4.1. The “mean” $M_{\text{HI}} - M_*$ scaling relation from HI 21 cm stacking and measurements of $\log \langle M_{\text{HI}} \rangle$

The $M_{\text{HI}} - M_*$ scaling relation in the local Universe is well described by a linear relation between the logarithm of the HI mass, $\log[M_{\text{HI}}]$, and the logarithm of the stellar mass, $\log[M_*]$ (e.g. Catinella et al. 2010, 2018; Parkash et al. 2018). Since measurements of the HI masses of individual galaxies are available in the nearby Universe, the best-fitting scaling relation is found using individual measurements of $\log[M_{\text{HI}}]$; this is the “standard” approach. Conversely, our stacking analysis at $z \sim 0.35$ yields the average HI mass of blue galaxies in different stellar mass bins, and does not yield measurements of the HI masses of individual galaxies. The scaling relations from such stacking analyses are hence obtained by fitting to measurements of $\log \langle M_{\text{HI}} \rangle$ in multiple stellar-mass bins (e.g. Brown et al. 2015; Chowdhury et al. 2022b). Thus, care must be taken when comparing the scaling relations from HI 21 cm stacking to those obtained from individual M_{HI} measurements at $z \approx 0$. In the present subsection, we will self-consistently compare scaling relations obtained by fits to measurements of $\log \langle M_{\text{HI}} \rangle$ at all redshifts; we will refer to this as the “mean” $M_{\text{HI}} - M_*$ scaling relation. The next subsection will discuss how one might determine the standard $M_{\text{HI}} - M_*$ scaling relation (referred to as the “median” $M_{\text{HI}} - M_*$ relation) via stacking analyses.

We followed the optimization approach of Chowdhury et al. (2022b) to determine the mean $M_{\text{HI}} - M_*$ scaling relation for blue galaxies at $z \approx 0.35$ from our measurements of the average HI masses in three stellar mass bins. We initially assume that the mean $M_{\text{HI}} - M_*$ relation can be written as

$$\log[M_{\text{HI}}/M_\odot] = m_9 + b [\log(M_*/M_\odot) - 9.0], \quad (4)$$

where b is the slope of the relation and m_9 is a normalization constant.⁷ For given values of b and m_9 , the HI mass of a galaxy, $M_{\text{HI}}([b, m_9]; M_*)$, can be obtained from its (known) stellar mass M_* using Equation 4. The average HI mass of galaxies in different stellar mass bins can be calculated from these individual HI masses. We denote the average HI mass of the i ’th stellar mass bin, corresponding to specific values of b and m_9 , by $\langle M_{\text{HI}} \rangle_i^{b, m_9}$. We find the best-fitting values of b and m_9 by minimizing the quantity

$$\chi^2 = \sum_i \frac{[\langle M_{\text{HI}} \rangle_i^{b, m_9} - \langle M_{\text{HI}} \rangle_i]^2}{[\Delta \langle M_{\text{HI}} \rangle_i]^2} \quad (5)$$

⁷ Note that we use this form of the scaling relation to minimize the covariance between the two fitted parameters of the $M_{\text{HI}} - M_*$ relation. Using the standard form $\log[M_{\text{HI}}/M_\odot] = \alpha + \beta * \log[M_*/M_\odot]$ (e.g. Catinella et al. 2018; Sinigaglia et al. 2022) gives a high covariance between α and β when fitting to a given narrow range of stellar masses.

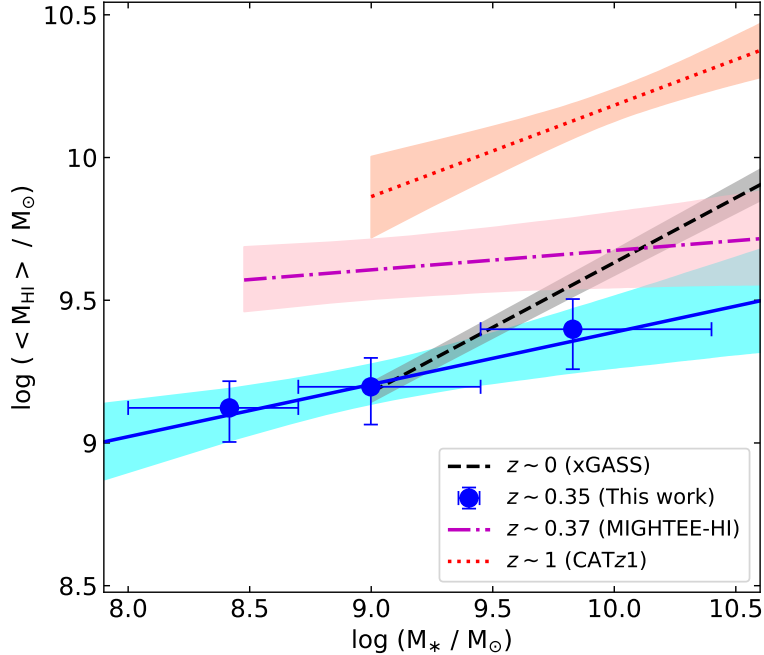


Figure 2. The $M_{\text{HI}} - M_*$ scaling relation, based on measurements of $\langle M_{\text{HI}} \rangle$ in blue star-forming galaxies: The blue filled circles show our HI 21 cm stacking measurements of $\log[\langle M_{\text{HI}} \rangle / M_\odot]$ in three (logarithmic) stellar-mass bins for blue galaxies at $z \sim 0.35$ in the EGS. The solid blue line is the best-fit mean $M_{\text{HI}} - M_*$ scaling relation, with the light blue shaded region showing the 68% confidence interval around the fit. The figure also shows the mean $M_{\text{HI}} - M_*$ scaling relations for blue star-forming galaxies at (1) $z \approx 0$ from the xGASS sample (dashed line; Catinella et al. 2018), (2) $z \approx 1$ from the GMRT-CATz1 survey (dotted line; Chowdhury et al. 2022a), and (3) at $z \approx 0.37$ from the MIGHTEE survey (dash-dotted line; Sinigaglia et al. 2022). Note that all scaling relations in the panel have been obtained by fitting a relation to the dependence of $\log \langle M_{\text{HI}} \rangle$ on M_* , and not to $\langle \log M_{\text{HI}} \rangle$, as is usually done at $z \approx 0$ (e.g. Catinella et al. 2018).

where $\langle M_{\text{HI}} \rangle_i$ is the measured average HI mass of galaxies in the i 'th bin and $\Delta \langle M_{\text{HI}} \rangle_i$ is the jackknife error on this quantity. Note that, in this method, any intrinsic scatter of the HI masses around the $M_{\text{HI}} - M_*$ scaling relation has been ignored (or, equivalently, assumed to be zero).

For blue galaxies at $z \sim 0.35$, we find that the best-fit mean $M_{\text{HI}} - M_*$ scaling relation is given by

$$\log[\langle M_{\text{HI}} \rangle / M_\odot] = (9.205 \pm 0.069) + (0.183 \pm 0.104) [\log(M_*/M_\odot) - 9.0], \quad (6)$$

which is shown as the blue solid line in Figure 2.

In the local Universe, Catinella et al. (2018) obtained the standard $M_{\text{HI}} - M_*$ scaling relation for the xGASS galaxy sample, using M_{HI} measurements in individual galaxies. To carry out a direct comparison to our scaling relation in Equation 6, we selected 592 blue galaxies from the xGASS sample (satisfying $\text{NUV} - r < 4$) and divided them in (logarithmic) stellar mass bins of width 0.2 dex.⁸ We then calculated the mean HI mass, $\langle M_{\text{HI}} \rangle$, for each stellar-mass bin, and estimated the associated uncertainty by jackknife resampling. Using these average HI masses and following the approach described above, we find that the best-fit mean $M_{\text{HI}} - M_*$ relation for blue xGASS galaxies is

$$\log[\langle M_{\text{HI}} \rangle / M_\odot] = (9.178 \pm 0.035) + (0.454 \pm 0.027) [\log(M_*/M_\odot) - 9.0]. \quad (7)$$

This relation is shown as the dashed line in Figure 2.

While comparing our scaling relation at $z \approx 0.35$ with that obtained from the xGASS sample at $z \approx 0$, it is important to emphasize that the stellar mass distributions of the two samples are different (as can be clearly seen in the stellar mass ranges of the two relations in Fig. 2). A comparison between the scaling relations requires us to assume that the xGASS relation may be extrapolated to lower stellar masses, $\approx 10^8 M_\odot$, and that the EGS relation is applicable at high stellar masses, $\approx 10^{11} M_\odot$.

⁸ We note that the xGASS sample only contains galaxies with $\log(M_*/M_\odot) > 9.0$ (Catinella et al. 2018).

With this assumption, we find that the normalization constants of the scaling relations at $z \sim 0.35$ and $z \sim 0$ are consistent within the errors, but the slopes are different at $\approx 2.5\sigma$ significance, with the relation at $z \sim 0.35$ being flatter than the local relation. This result indicates that massive star-forming galaxies with $M_* \gtrsim 10^{10} M_\odot$ are relatively HI-poor compared to their local counterparts. Conversely, low-mass star-forming galaxies at $z \approx 0.35$, with $M_* < 10^{8.5} M_\odot$, appear to be HI-rich compared to similar galaxies at $z \approx 0$.

The dotted line in Fig. 2 shows the mean $M_{\text{HI}} - M_*$ scaling relation at $z \approx 1$, obtained from HI 21 cm stacking with the GMRT-CATz1 survey (Chowdhury et al. 2022a,b). The slope of the scaling relation at $z \approx 1$ is formally intermediate between the values at $z \approx 0.35$ (obtained here) and $z \approx 0$, albeit consistent with both, within the errors (we again assume that each scaling relation may be extrapolated to the stellar mass range of the other relations). However, the normalization of the relation is significantly higher at $z \approx 1$, by ≈ 0.6 dex at $M_* \approx 10^{10} M_\odot$. This indicates that star-forming galaxies at $z \approx 1$ are ≈ 3.5 times more gas-rich than galaxies of similar stellar masses at $z \approx 0.35$ and $z \approx 0$ (Chowdhury et al. 2022b).

Recently, Sinigaglia et al. (2022) used a similar HI 21 cm stacking approach with MeerKAT observations of the COSMOS field to measure the mean $M_{\text{HI}} - M_*$ scaling relation for star-forming galaxies at $z \approx 0.37$. We used their average HI mass measurements in different stellar mass bins (kindly provided by F. Sinigaglia) to obtain the best-fit scaling relation of the form given in Equation 4. This yields $\log[\langle M_{\text{HI}} \rangle / M_\odot] = (9.61 \pm 0.11) + (0.068 \pm 0.078) [\log(M_*/M_\odot) - 9.0]$ at $z \approx 0.37$. Figure 2 compares our $M_{\text{HI}} - M_*$ relation (blue solid line) with that of Sinigaglia et al. (2022) (dash-dotted line). The scaling relation of Sinigaglia et al. (2022) is seen to lie above our relation (by ≈ 0.4 dex at $M_* \approx 10^9 M_\odot$), with an $\approx 3\sigma$ difference in the normalization of the relation. Finally, while the slope of the COSMOS scaling relation in Fig. 2 appears flatter than that of the EGS scaling relation, the two slopes are formally consistent within the errors.

Our present measurement has a normalization similar to that of the relation at $z \approx 0$ (from the xGASS sample), while the relation of Sinigaglia et al. (2022) lies above the local relation. The two scaling relations have different implications for the evolution of gas in galaxies from $z \approx 1$ to the present epoch. We emphasize that the scaling relation obtained here, from the EGS, is based on a relatively small cosmic volume ($\approx 4.7 \times 10^4$ comoving Mpc³) and a small number of galaxies (≈ 500 objects), implying that cosmic variance could affect our results. However, the detection significance in each stellar-mass bin is relatively high, with $> 4\sigma$ significance. Conversely, the result of Sinigaglia et al. (2022) is based on a far larger sample (≈ 9000 galaxies) and a larger cosmic volume ($\approx 8.5 \times 10^5$ comoving Mpc³, albeit still significantly affected by cosmic variance; e.g. Driver & Robotham 2010). However, there are clear systematic effects in the stacked HI 21 cm spectra of Sinigaglia et al. (2022), including oscillations in both the full stacked spectrum and the reference spectrum of their Fig. 2, an absorption feature stronger than the emission feature in the top middle spectrum of their Fig. 3, etc, and the detection significance of the stacked HI 21 cm emission signal is low ($\approx 3\sigma$) in some bins. All of these make the results less reliable. In addition, Sinigaglia et al. (2022) do not exclude objects identified as AGNs from their sample ($\approx 3.5\%$ of their galaxies); this too could affect the slope of the $M_{\text{HI}} - M_*$ relation, if AGNs predominantly arise in more massive galaxies. Overall, a combination of deeper and wider HI 21 cm stacking observations is critically needed to accurately determine the shape of the $M_{\text{HI}} - M_*$ relation at intermediate redshifts and to trace the evolution of HI in galaxies from $z \approx 1$ to today.

4.2. The “median” $M_{\text{HI}} - M_*$ scaling relation from HI 21 cm stacking and estimates of $\langle \log M_{\text{HI}} \rangle$

In the previous subsection, we presented the mean $M_{\text{HI}} - M_*$ scaling relation obtained by fitting to the $\log \langle M_{\text{HI}} \rangle$ values that are measured in HI 21 cm stacking studies. As noted earlier, in the local Universe, one usually determines the $M_{\text{HI}} - M_*$ relation by fitting to measurements of the stellar mass and the HI mass of individual galaxies; this is effectively the same as fitting to measurements of $\langle \log M_{\text{HI}} \rangle$. For the blue galaxies of the xGASS sample, the best-fit $M_{\text{HI}} - M_*$ relation obtained by this approach is (Catinella et al. 2018)

$$\log(M_{\text{HI}}/M_\odot) = (8.934 \pm 0.036) + (0.516 \pm 0.030) [\log(M_*/M_\odot) - 9.0] \quad (8)$$

This scaling relation has a logarithmic scatter of $\sigma = 0.445$ dex (Catinella et al. 2018).

A comparison between Equations 7 and 8 shows that the slopes of the two $M_{\text{HI}} - M_*$ relations at $z \approx 0$ are in excellent agreement, but that the former relation lies ≈ 0.25 dex above the latter one. This is to be expected when there is an intrinsic scatter in the HI masses in each stellar-mass bin: for a symmetric logarithmic scatter in the HI masses, the relation in Equation 7 traces the logarithm of the average HI mass in each stellar-mass bin, while the relation in Equation 8 traces the logarithm of the median HI mass in each bin (Bera et al. 2022). We will hence refer

to the standard $M_{\text{HI}} - M_*$ scaling relation, obtained by fitting to measurements of the HI mass and the stellar mass in individual galaxies, as the median $M_{\text{HI}} - M_*$ relation.

As noted by Bera et al. (2022), one needs to know the intrinsic scatter in the $M_{\text{HI}} - M_*$ relation in order to determine the median $M_{\text{HI}} - M_*$ relation from the mean $M_{\text{HI}} - M_*$ relation. Unfortunately, this information on the intrinsic scatter in the $M_{\text{HI}} - M_*$ relation is not presently available beyond the local Universe.

To determine the median $M_{\text{HI}} - M_*$ relation at $z \approx 0.35$ from our measurements of the average HI masses in the different stellar mass bins, we assume that the HI masses of individual blue galaxies in each stellar-mass bin at $z \sim 0.35$ are lognormally distributed, with the same intrinsic scatter as that of blue xGASS galaxies at $z \approx 0$. In other words, we assume that the intrinsic scatter in the $M_{\text{HI}} - M_*$ relation for blue galaxies at $z \approx 0.35$ is $\sigma = 0.445$ dex, the same as that in the local Universe. Bera et al. (2022) show that the ratio of the mean HI mass to the median HI mass for a sample of galaxies can be used to obtain an upper limit to the intrinsic lognormal scatter in the $M_{\text{HI}} - M_*$ relation. For our 464 blue galaxies at $z \approx 0.35$, the mean HI mass is $(1.57 \pm 0.26) \times 10^9 M_\odot$, while the median HI mass is $(1.17 \pm 0.22) \times 10^9 M_\odot$. Following Bera et al. (2022), we then obtain the upper limit $\sigma_{\text{max}} = 0.33 \pm 0.10$ dex, which is consistent with the assumed scatter of 0.445 dex.

For a lognormal distribution of HI masses, with an intrinsic scatter σ , the logarithm of the mean of the distribution and the mean of the logarithm of individual HI masses are related by

$$\log \langle M_{\text{HI}} \rangle - \langle \log M_{\text{HI}} \rangle = \frac{\ln 10}{2} \sigma^2 \quad (9)$$

The best-fit median $M_{\text{HI}} - M_*$ scaling relation can hence be obtained by combining Equations 6 and 9; this gives

$$\log (M_{\text{HI}}/M_\odot) = (8.977 \pm 0.069) + (0.183 \pm 0.104) [\log(M_*/M_\odot) - 9.0]. \quad (10)$$

In passing, we note that a very similar relation is obtained by explicitly carrying out a least-squares fit via Equation 5, but this time including the intrinsic lognormal scatter of 0.445 dex.

We emphasize that the derivation of the median $M_{\text{HI}} - M_*$ relation in Equation 10 makes the critical assumptions that the intrinsic scatter of HI masses in each stellar-mass bin follows a lognormal distribution, and that the intrinsic scatter is the same as that in the local Universe. The mean $M_{\text{HI}} - M_*$ relation of Equation 6 does not make these assumptions, and is thus a more general relation from HI 21 cm stacking studies.

5. THE HI DEPLETION TIMESCALE

The HI depletion timescale ($t_{\text{dep}} \equiv M_{\text{HI}}/\text{SFR}$) of a galaxy gives the timescale over which its HI mass would be completely consumed at its current SFR (with an intermediate conversion to molecular hydrogen). t_{dep} is thus a measure of how long a galaxy can sustain its star-formation activity without replenishment of its HI reservoir. Its inverse is a measure of the current star-formation efficiency of a galaxy, relative to its HI content. In the local Universe, the HI depletion timescale has been found to show only a weak dependence on the stellar mass (e.g. Schiminovich et al. 2010; Saintonge et al. 2017).

As noted earlier, HI 21 cm stacking studies yield direct measurements of the average HI mass of galaxy samples. One can combine these average HI masses with the average SFRs of the same samples to obtain the *characteristic* HI depletion timescale, $\langle t_{\text{dep}} \rangle \equiv \langle M_{\text{HI}} \rangle / \langle \text{SFR} \rangle$, of the sample. We emphasize that the characteristic HI depletion timescale is not the same as the average HI depletion timescale, $\langle M_{\text{HI}} / \text{SFR} \rangle$ (e.g. Chowdhury et al. 2022b).

The dependence of the characteristic HI depletion timescale on the stellar mass can be obtained by combining Equation 6 with the main-sequence relation of star-forming galaxies (e.g. Brinchmann et al. 2004; Noeske et al. 2007; Whitaker et al. 2012). At $z = 0.35$, the median redshift of our galaxy sample, the main sequence is well described by the relation (Whitaker et al. 2012)

$$\log (\text{SFR}/M_\odot \text{ yr}^{-1}) = 0.65 [\log (M_*/M_\odot) - 10.5] + 0.76. \quad (11)$$

Dividing Equation 6 by Equation 11, we find that the characteristic HI depletion timescale for blue galaxies at $z \sim 0.35$ is given by

$$\log [\langle t_{\text{dep}} \rangle / \text{Gyr}] = (0.420 \pm 0.069) - (0.467 \pm 0.104) [\log(M_*/M_\odot) - 9.0]. \quad (12)$$

Note that the uncertainties in this relation do not include the uncertainties in the slope and the normalization of the main-sequence relation (Equation 11).

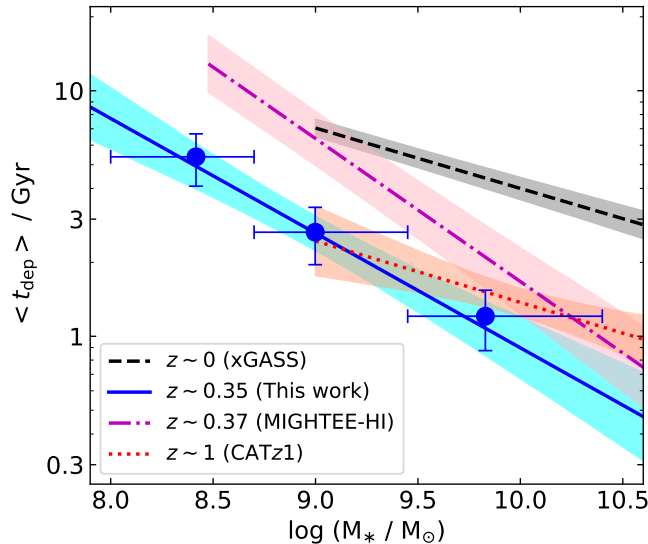


Figure 3. The characteristic HI depletion timescale as a function of stellar mass at different redshifts: The blue circles show the measurements of the characteristic HI depletion times for blue galaxies at $z \approx 0.35$ for three stellar mass bins, while the blue solid line and shaded region show, respectively, the $t_{\text{dep}} - M_*$ scaling relation and the 68% confidence interval for these galaxies. The figure also shows the characteristic HI depletion timescales for blue star-forming galaxies at (1) $z \approx 0$ from the xGASS sample (dashed black line; Catinella et al. 2018), (2) $z \approx 1$ from the GMRT-CATz1 survey (dotted red line; Chowdhury et al. 2022a), and (3) $z \approx 0.37$ from the MIGHTEE-HI survey (dash-dotted magenta line; Sinigaglia et al. 2022). Note that all scaling relations in the panel have been obtained uniformly by combining the $\log \langle M_{\text{HI}} \rangle - \log M_*$ relation with the (redshift-dependent) main-sequence relation from Whitaker et al. (2012).

Following a similar approach, we estimated the characteristic HI depletion timescales for blue star-forming galaxies at $z \approx 0$ and $z \approx 1$, by combining the corresponding $M_{\text{HI}} - M_*$ scaling relation with the (redshift-dependent) main-sequence relation (Whitaker et al. 2012). We obtain, for blue galaxies in the xGASS sample at $z \approx 0$ (Catinella et al. 2018)

$$\log [\langle t_{\text{dep}} \rangle / \text{Gyr}] = (0.848 \pm 0.035) - (0.246 \pm 0.027) [\log(M_*/M_\odot) - 9.0], \quad (13)$$

while, for blue galaxies at $z \approx 1$ from the GMRT-CATz1 survey (Chowdhury et al. 2022a),⁹

$$\log [\langle t_{\text{dep}} \rangle / \text{Gyr}] = (0.138 \pm 0.056) - (0.25 \pm 0.13) [\log(M_*/M_\odot) - 10.0]. \quad (14)$$

Figure 3 compares the $\langle t_{\text{dep}} \rangle - M_*$ relation obtained from our observations of the EGS (solid blue line) with the relations obtained at $z \approx 1$ (dotted line) and $z \approx 0$ (dashed line). The shaded regions indicate the 68% confidence interval around each relation. We find that the characteristic HI depletion timescales of star-forming galaxies (with $M_* > 10^9 M_\odot$) at $z \sim 0.35$ are lower by a factor of $\approx 3 - 5$ compared to those of galaxies with similar stellar masses at the present epoch. However, the characteristic HI depletion timescales of blue galaxies at $z \sim 0.35$ in the EGS are comparable to those of blue galaxies of similar stellar masses at $z \sim 1$ (Chowdhury et al. 2022a). Our current results thus suggest that the star-formation efficiency (relative to HI) of blue star-forming galaxies did not evolve significantly over the ≈ 4 Gyr from $z \approx 1$ to $z \approx 0.35$, but declined steeply over the next ≈ 4 Gyr, from $z \approx 0.35$ to $z \approx 0$.

Figure 3 shows that star-forming galaxies at $z \approx 0.35$, roughly 4 Gyr ago, with $M_* \gtrsim 10^9 M_\odot$ have characteristic HI depletion timescales lower than ≈ 3 Gyr. Such galaxies would entirely consume their HI reservoirs much before the present epoch. This would result in quenching of their star-formation activity, unless they accrete significant amounts of gas from the circumgalactic medium (CGM) over the past 4 Gyr, to replenish their HI reservoirs. This is a very interesting result, although we again emphasize that it is based on observations of a relatively small cosmic volume ($\approx 4.7 \times 10^4$ comoving Mpc³), and hence may be affected by cosmic variance.

⁹ We note that Chowdhury et al. (2022b) use a second-order form of the main-sequence relation, from Whitaker et al. (2014), to obtain the $\langle t_{\text{dep}} \rangle - M_*$ relation at $z \approx 1$.

Figure 3 also shows the characteristic HI depletion timescale at $z \approx 0.37$ (dash-dotted line) obtained using the $M_{\text{HI}} - M_*$ scaling relation from the MIGHTEE-HI survey (Sinigaglia et al. 2022). This yields $\log [\langle t_{\text{dep}} \rangle / \text{Gyr}] = (0.81 \pm 0.11) - (0.582 \pm 0.078) [\log(M_*/M_\odot) - 9.0]$. We find that the MIGHTEE-HI $\langle t_{\text{dep}} \rangle - M_*$ relation has a slope similar to ours, but a higher normalization, by a factor of ≈ 2.5 . The discrepancy is due to the difference in the two “mean” $M_{\text{HI}} - M_*$ relations, discussed in the previous section. As noted earlier, a combination of deep and wide HI 21 cm stacking observations is critical to resolve this issue.

6. SUMMARY

We have used a GMRT HI 21 cm survey of the Extended Groth Strip, and the technique of HI 21 cm stacking, to measure the scaling relation between the HI mass and the stellar mass for blue star-forming galaxies at $z \approx 0.35$. We have also combined our estimate of the $M_{\text{HI}} - M_*$ relation with the main-sequence relation for star-forming galaxies at $z \approx 0.35$ to determine the dependence of the characteristic HI depletion timescale of star-forming galaxies on their stellar mass. We find that massive star-forming galaxies at $z \approx 0.35$, with $M_* \gtrsim 10^{10} M_\odot$, are relatively HI-poor compared to local star-forming galaxies of similar stellar mass. However, the HI-based star-formation efficiency of massive galaxies at $z \approx 0.35$ is higher by a factor of ≈ 5 compared to that of their local counterparts.

The $M_{\text{HI}} - M_*$ scaling relation obtained in our study of the EGS at $z \approx 0.35$ is different (at $\approx 3\sigma$ significance) from that obtained by Sinigaglia et al. (2022) at $z \approx 0.37$ from a similar HI 21 cm stacking analysis applied to MIGHTEE-HI observations of the COSMOS field. Both studies stack the HI 21 cm signals from star-forming galaxies on the main sequence; the difference between the scaling relations is unlikely to arise from differences in the sample or the approaches to determine the M_* estimates (although we note that, unlike the present study, Sinigaglia et al. (2022) retain AGNs in their sample). The difference between the two results is likely to arise due to a combination of systematic errors and low significance measurements affecting the spectra of Sinigaglia et al. (2022) and cosmic variance affecting both studies due to their relatively small cosmic volumes.

While our results are based on a small cosmic volume and could thus be affected by cosmic variance, the short inferred characteristic HI depletion timescales ($\lesssim 3$ Gyr) of star-forming galaxies at $z \approx 0.35$ with stellar masses $\gtrsim 10^9 M_*$ imply that such galaxies must have acquired significant amounts of neutral gas through accretion from the CGM over the past four Gyr to prevent quenching of their star-formation activity.

1 We thank an anonymous referee for detailed comments on an earlier version of this paper. We thank the staff of the
2 GMRT who have made these observations possible. The GMRT is run by the National Centre for Radio Astrophysics
3 of the Tata Institute of Fundamental Research. We are grateful to Francesco Sinigaglia for providing us with the
4 average HI and average stellar masses in the different bins of their MIGHTEE-HI study, and to Ben Weiner for
5 providing us with the $H\alpha$ and $H\beta$ line luminosities of the DEEP2 galaxies. AB and NK thank Aditya Chowdhury
6 for many discussions on HI 21 cm stacking that have contributed to this paper. NK acknowledges support from the
7 Department of Science and Technology via a Swarnajayanti Fellowship (DST/SJF/PSA-01/2012-13). AB, NK, & JNC
8 also acknowledge the Department of Atomic Energy for funding support, under project 12-R&D-TFR-5.02-0700.

REFERENCES

- Aditya, J. N. H. S., & Kanekar, N. 2018, *MNRAS*, 481, 1578, doi: [10.1093/mnras/sty2184](https://doi.org/10.1093/mnras/sty2184)
- Bera, A. 2021, PhD thesis, TIFR Deemed-to-be University, India
- Bera, A., Kanekar, N., Chengalur, J. N., & Bagla, J. S. 2019, *The Astrophysical Journal Letters*, 882, L7, doi: [10.3847/2041-8213/ab3656](https://doi.org/10.3847/2041-8213/ab3656)
- . 2022, *The Astrophysical Journal Letters*, 940, L10, doi: [10.3847/2041-8213/ac9d32](https://doi.org/10.3847/2041-8213/ac9d32)
- . in prep.
- Briggs, D. S. 1995, in *American Astronomical Society Meeting Abstracts*, Vol. 187, American Astronomical Society Meeting Abstracts, 112.02
- Brinchmann, J., Charlot, S., White, S. D. M., et al. 2004, *MNRAS*, 351, 1151, doi: [10.1111/j.1365-2966.2004.07881.x](https://doi.org/10.1111/j.1365-2966.2004.07881.x)
- Broeils, A. H., & Rhee, M. H. 1997, *A&A*, 324, 877
- Brown, T., Catinella, B., Cortese, L., et al. 2015, *MNRAS*, 452, 2479, doi: [10.1093/mnras/stv1311](https://doi.org/10.1093/mnras/stv1311)
- Catinella, B., & Cortese, L. 2015, *MNRAS*, 446, 3526, doi: [10.1093/mnras/stu2241](https://doi.org/10.1093/mnras/stu2241)
- Catinella, B., Schiminovich, D., Kauffmann, G., et al. 2010, *MNRAS*, 403, 683, doi: [10.1111/j.1365-2966.2009.16180.x](https://doi.org/10.1111/j.1365-2966.2009.16180.x)
- Catinella, B., Saintonge, A., Janowiecki, S., et al. 2018, *MNRAS*, 476, 875, doi: [10.1093/mnras/sty089](https://doi.org/10.1093/mnras/sty089)
- Chengalur, J. N., Braun, R., & Wieringa, M. 2001, *A&A*, 372, 768, doi: [10.1051/0004-6361:20010547](https://doi.org/10.1051/0004-6361:20010547)
- Chowdhury, A., Kanekar, N., & Chengalur, J. N. 2022a, *ApJ*, 937, 103. <https://arxiv.org/abs/2207.00031>
- . 2022b, *ApJL*, 941, L6, doi: [10.3847/2041-8213/ac9d8a](https://doi.org/10.3847/2041-8213/ac9d8a)
- Chowdhury, A., Kanekar, N., Das, B., Dwarakanath, K. S., & Sethi, S. 2021, *ApJL*, 913, L24, doi: [10.3847/2041-8213/abfcc7](https://doi.org/10.3847/2041-8213/abfcc7)
- Coil, A. L., Newman, J. A., Croton, D., et al. 2008, *ApJ*, 672, 153, doi: [10.1086/523639](https://doi.org/10.1086/523639)
- Condon, J. J., Cotton, W. D., & Broderick, J. J. 2002, *AJ*, 124, 675, doi: [10.1086/341650](https://doi.org/10.1086/341650)
- Cooper, M. C., Griffith, R. L., Newman, J. A., et al. 2012, *MNRAS*, 419, 3018, doi: [10.1111/j.1365-2966.2011.19938.x](https://doi.org/10.1111/j.1365-2966.2011.19938.x)
- Cornwell, T. J., Golap, K., & Bhatnagar, S. 2008, *IEEE Journal of Selected Topics in Signal Processing*, 2, 647, doi: [10.1109/JSTSP.2008.2005290](https://doi.org/10.1109/JSTSP.2008.2005290)
- Davé, R., Crain, R. A., Stevens, A. R. H., et al. 2020, *MNRAS*, 497, 146, doi: [10.1093/mnras/staa1894](https://doi.org/10.1093/mnras/staa1894)
- Davis, T. A., Young, L. M., Crocker, A. F., et al. 2014, *MNRAS*, 444, 3427, doi: [10.1093/mnras/stu570](https://doi.org/10.1093/mnras/stu570)
- Dénes, H., Kilborn, V. A., & Koribalski, B. S. 2014, *MNRAS*, 444, 667, doi: [10.1093/mnras/stu1337](https://doi.org/10.1093/mnras/stu1337)
- Driver, S. P., & Robotham, A. S. G. 2010, *MNRAS*, 407, 2131, doi: [10.1111/j.1365-2966.2010.17028.x](https://doi.org/10.1111/j.1365-2966.2010.17028.x)
- Fernández, X., Gim, H. B., van Gorkom, J. H., et al. 2016, *ApJL*, 824, L1, doi: [10.3847/2041-8205/824/1/L1](https://doi.org/10.3847/2041-8205/824/1/L1)
- Gogate, A. R., Verheijen, M. A. W., Deshev, B. Z., et al. 2020, *MNRAS*, 496, 3531, doi: [10.1093/mnras/staa1680](https://doi.org/10.1093/mnras/staa1680)
- Greisen, E. W. 2003, in *Astrophysics and Space Science Library*, Vol. 285, *Information Handling in Astronomy - Historical Vistas*, ed. A. Heck (Kluwer Academic Publishers; Dordrecht), 109, doi: [10.1007/0-306-48080-8_7](https://doi.org/10.1007/0-306-48080-8_7)
- Hopkins, A. M., Miller, C. J., Nichol, R. C., et al. 2003, *ApJ*, 599, 971, doi: [10.1086/379608](https://doi.org/10.1086/379608)
- Jaffé, Y. L., Verheijen, M. A. W., Haines, C. P., et al. 2016, *MNRAS*, 461, 1202, doi: [10.1093/mnras/stw984](https://doi.org/10.1093/mnras/stw984)
- Maddox, N., Hess, K. M., Blyth, S. L., & Jarvis, M. J. 2013, *MNRAS*, 433, 2613, doi: [10.1093/mnras/stt934](https://doi.org/10.1093/mnras/stt934)
- McMullin, J. P., Waters, B., Schiebel, D., Young, W., & Golap, K. 2007, in *Astronomical Society of the Pacific Conference Series*, Vol. 376, *Astronomical Data Analysis Software and Systems XVI*, ed. R. A. Shaw, F. Hill, & D. J. Bell, 127
- Morganti, R., & Oosterloo, T. 2018, *A&A Rv*, 26, 4, doi: [10.1007/s00159-018-0109-x](https://doi.org/10.1007/s00159-018-0109-x)
- Morganti, R., Veilleux, S., Oosterloo, T., Teng, S. H., & Rupke, D. 2016, *A&A*, 593, A30, doi: [10.1051/0004-6361/201628978](https://doi.org/10.1051/0004-6361/201628978)
- Newman, J. A., Cooper, M. C., Davis, M., et al. 2013, *ApJS*, 208, 5, doi: [10.1088/0067-0049/208/1/5](https://doi.org/10.1088/0067-0049/208/1/5)
- Noeske, K. G., Weiner, B. J., Faber, S. M., et al. 2007, *ApJL*, 660, L43, doi: [10.1086/517926](https://doi.org/10.1086/517926)
- Oke, J. B. 1974, *ApJS*, 27, 21, doi: [10.1086/190287](https://doi.org/10.1086/190287)
- Parkash, V., Brown, M. J. I., Jarrett, T. H., & Bonne, N. J. 2018, *ApJ*, 864, 40, doi: [10.3847/1538-4357/aad3b9](https://doi.org/10.3847/1538-4357/aad3b9)
- Rupke, D. S. N., & Veilleux, S. 2011, *ApJL*, 729, L27, doi: [10.1088/2041-8205/729/2/L27](https://doi.org/10.1088/2041-8205/729/2/L27)
- Saintonge, A., & Catinella, B. 2022, *ARA&A*, 60, 319, doi: [10.1146/annurev-astro-021022-043545](https://doi.org/10.1146/annurev-astro-021022-043545)
- Saintonge, A., Catinella, B., Tacconi, L. J., et al. 2017, *ApJS*, 233, 22, doi: [10.3847/1538-4365/aa97e0](https://doi.org/10.3847/1538-4365/aa97e0)
- Schiminovich, D., Catinella, B., Kauffmann, G., et al. 2010, *MNRAS*, 408, 919, doi: [10.1111/j.1365-2966.2010.17210.x](https://doi.org/10.1111/j.1365-2966.2010.17210.x)
- Serra, P., Oosterloo, T., Morganti, R., et al. 2012, *MNRAS*, 422, 1835, doi: [10.1111/j.1365-2966.2012.20219.x](https://doi.org/10.1111/j.1365-2966.2012.20219.x)
- Sinigaglia, F., Rodighiero, G., Elson, E., et al. 2022, *ApJL*, 935, L13, doi: [10.3847/2041-8213/ac85ae](https://doi.org/10.3847/2041-8213/ac85ae)
- Smolčić, V., Schinnerer, E., Scodreggio, M., et al. 2008, *ApJS*, 177, 14, doi: [10.1086/588028](https://doi.org/10.1086/588028)

- Stefanon, M., Yan, H., Mobasher, B., et al. 2017, ApJS, 229, 32, doi: [10.3847/1538-4365/aa66cb](https://doi.org/10.3847/1538-4365/aa66cb)
- Toribio, M. C., Solanes, J. M., Giovanelli, R., Haynes, M. P., & Martin, A. M. 2011, ApJ, 732, 93, doi: [10.1088/0004-637X/732/2/93](https://doi.org/10.1088/0004-637X/732/2/93)
- Wang, J., Koribalski, B. S., Serra, P., et al. 2016, MNRAS, 460, 2143, doi: [10.1093/mnras/stw1099](https://doi.org/10.1093/mnras/stw1099)
- Weiner, B. J., Coil, A. L., Prochaska, J. X., et al. 2009, ApJ, 692, 187, doi: [10.1088/0004-637X/692/1/187](https://doi.org/10.1088/0004-637X/692/1/187)
- Whitaker, K. E., van Dokkum, P. G., Brammer, G., & Franx, M. 2012, ApJL, 754, L29, doi: [10.1088/2041-8205/754/2/L29](https://doi.org/10.1088/2041-8205/754/2/L29)
- Whitaker, K. E., Franx, M., Leja, J., et al. 2014, ApJ, 795, 104, doi: [10.1088/0004-637X/795/2/104](https://doi.org/10.1088/0004-637X/795/2/104)
- Willmer, C. N. A., Faber, S. M., Koo, D. C., et al. 2006, ApJ, 647, 853, doi: [10.1086/505455](https://doi.org/10.1086/505455)
- Zwaan, M. A. 2000, PhD thesis, University of Groningen, The Netherlands